



ELSEVIER

Physica C 308 (1998) 123–131

PHYSICA C

## The effect of sample shape on the magnetisation in $\text{Bi}_2\text{Sr}_2\text{CaCu}_2\text{O}_{8+\delta}$ crystals

R.A. Doyle <sup>a,\*</sup>, S.F.W.R. Rycroft <sup>a</sup>, C.D. Dewhurst <sup>a,1</sup>, E. Zeldov <sup>b</sup>, I. Tsabba <sup>c</sup>,  
S. Reich <sup>c</sup>, T.B. Doyle <sup>d</sup>, T. Tamegai <sup>e</sup>, S. Ooi <sup>e</sup>

<sup>a</sup> *IRC in Superconductivity, University of Cambridge, West Cambridge Site, Madingley Road, Cambridge, CB3 0HE, UK*

<sup>b</sup> *Department of Condensed Matter Physics, Weizmann Institute of Science, Rehovot 76100, Israel*

<sup>c</sup> *Department of Materials and Interfaces, Weizmann Institute of Science, Rehovot 76100, Israel*

<sup>d</sup> *Department of Physics, University of Natal Durban, King George V Avenue, Durban 4000, South Africa*

<sup>e</sup> *Department of Applied Physics, University of Tokyo, Bunkyo-ku, Tokyo 113-8656, Japan*

Received 24 July 1998; accepted 29 August 1998

### Abstract

Magnetic moment measurements have been made on differently shaped single crystals of  $\text{Bi}_2\text{Sr}_2\text{CaCu}_2\text{O}_{8+\delta}$  using a SQUID magnetometer. In platelet shaped samples, the results show a pronounced geometrical barrier (GB) or ‘shape effect’ at low fields and high temperatures. In both prism and semi-ellipsoidal-shaped samples, the low field magnetic hysteresis is reduced significantly at high temperatures due to modification of the geometrical barrier. At lower temperatures, the prism and semi-ellipsoidal samples show enhanced low field hysteresis relative to the platelet, suggesting an increasing role of nongeometrical surface barriers (SB). These results are discussed in terms of the competing roles of bulk pinning, surface and geometrical barrier effects. © 1998 Elsevier Science B.V. All rights reserved.

PACS: 74.60 Fc; 74.60 Ge; 74.60 Jg

Keywords: BSCCO; Melting; Irreversibility line; Geometrical barrier; Surface barrier; Bulk pinning

### 1. Introduction

The  $\text{Bi}_2\text{Sr}_2\text{CaCu}_2\text{O}_{8+\delta}$  (BSCCO) high temperature superconductor has extreme anisotropy and very low levels of bulk pinning at high temperatures (i.e.,

> 70 K). Single crystals of this material are invariably produced in the form of platelets with very large aspect ratios. Since most magnetic and transport measurements are carried out with the applied field parallel to the *c*-axis, i.e., parallel to the shortest dimension of the platelets, demagnetising effects are important and complicated by the nonellipsoidal geometry. The unusual material properties and sample geometry conspire to make all relevant energy scales (i.e., pinning, thermal, elastic and surface-related) in the mixed state comparable at higher tem-

\* Corresponding author. Tel.: +44-1223-337072; Fax: +44-1223-33074; E-mail: rad1005@hermes.cam.ac.uk

<sup>1</sup> Present address: Department of Physics, University of Warwick, Coventry CV4 7AL, UK.

peratures [1,2]. Accordingly, bulk pinning [3–12], geometrical barriers (GB) [5–12] and surface barriers (SB) [13–20] [21–24] may all contribute significantly to hysteresis in the global magnetisation. When bulk pinning predominates, the magnetisation curves do not display a sharp initial vortex penetration peak. The  $M$ - $H$  loops are symmetric about the reversible magnetisation behaviour and a significant remnant moment is apparent. Near  $T_c$  in both  $\text{YBa}_2\text{Cu}_3\text{O}_{7-\delta}$  (YBCO) and BSCCO, bulk pinning is very weak [8,24] and contributions to magnetically determined hysteresis from surface or geometrical barriers dominate, thus making the interpretation of magnetic behaviour in terms of bulk properties very complicated.

The geometrical barrier is a result of nonellipsoidal sample geometry and is strongest for samples with large aspect ratios and with the field parallel to the short axis. The energy of a vortex depends, in this geometry, on its position in the specimen because of magnetostatic effects, i.e., demagnetisation inhomogeneity. A rigorous description of the geometrical barrier in terms of continuum mechanics has recently been developed [25] while an equally rigorous thermodynamic description is presented in Ref. [26]. The latter paper, in particular, addresses the role of vortices and line tension in the thermodynamic description. As discussed in these papers, the geometrical barrier results in vortices first penetrating diagonally across the corners of the specimen [5–11] and leads to a delayed penetration field. The gradient in magnetic potential that the vortices experience once they have penetrated then drives them to the centre of the sample at a rate determined by the absence of pinning and viscous forces. Here, they concentrate in a ‘pool’ with a profile, in increasing field, which is ‘dome-like’ with a flat maximum in the sample centre and which grows in increasing field in the range  $0 < H_a < 0.5H_{c1}$ . With decreasing field, the profile must obviously expand to fill the specimen in order for flux to be able to exit the sample. This process leads to strong hysteresis in the magnetisation, even in the complete absence of pinning, for fields  $0 < H_a < 0.5H_{c1}$  [5]. Complicated edge effects can extend its influence, in diminished value, to much larger fields [7]. Note that the GB is determined entirely by the reversible magnetisation and the satisfaction of magnetic boundary conditions.

It is therefore not subject to the effects of thermal activation.

There are many different types of surface barriers and a good review is given in Ref. [13]. Surface barriers, unlike geometrical barriers, arise from a competition between the Lorentz force of the Meissner (London) screening current that drives vortices into the sample and the attractive interaction between vortices and their image at a sample surface. The standard description of the Bean–Livingstone barrier considers the case of a vortex penetrating through a smooth parallel surface. This type of barrier is expected to be suppressed by sharp corners. In HTS, the situation may be different because the vortices can be considered as stacks of pancake vortices rather than a continuous vortex line. The surface barriers are proposed to act on single pancakes in this case [17,18] and the barriers are expected to be enhanced. Within this scenario, displacement of a vortex that lies parallel to the  $c$ -axis, in a shaped sample where the surface has a component normal to the vortex, always requires additional pancakes to be added or lost from the vortex. A different but equivalent description is that this 2D ‘distributed’ surface barrier acts on all vortices and for all vortex motion for samples where the large surfaces are not parallel and strictly orthogonal to the field direction. Like geometrical barriers, the surface barrier results in a delayed initial penetration field and in magnetic hysteresis in the absence of bulk pinning, for fields up to the thermodynamic critical field,  $H_c$ . In both cases, magnetisation loops are usually strongly asymmetric about the reversible behaviour. The returning leg in decreasing field is typically flat and is close to zero for surface barriers since there is no barrier to flux exit (in the case of HTS) as the magnetisation,  $M$ , crosses through zero. In both cases of the (SB) and GB, in the absence of any bulk pinning, no remnant moment is expected. The surface barrier differs from the geometrical barrier in a number of respects. It acts on a microscopic scale and is subject to thermal activation, resulting in a time-dependence of the first penetration field,  $H_p(T)$ , and an exponential dependence [17,18] of this field on temperature,  $H_p(T) = H_p(0)\exp(-T/T_0)$  where  $T_0$  is typically 25 K. In principle, this difference should be sufficient to distinguish between the two types of barrier. In practice, because bulk pinning is also a thermally acti-

vated process, a combination of weak pinning and a geometrical barrier may manifest in many of the same features as the surface barrier.

The similarities and differences between the GB and SB, and the difficulties of separating these, have been discussed at length by van der Beek et al. [14] who have used an ac screening technique to try to separate bulk and surface- or geometry-related contributions. A different approach, which is the one we employ here, is to change the sample geometry. This modifies the demagnetising factor and internal field distribution. If, as proposed [17,18], the surface barriers are 2D in nature they should not be sensitive to the sample geometry. Thus, provided the polishing process does not induce defects that change bulk pinning considerably, this approach should assist in elucidating the mechanisms controlling hysteresis. This has important implications for the correct identification of the lower critical field, bulk-pinning related irreversibility line and critical current values. Surprisingly, few reports on shape modification have appeared in the literature. Majer et al. [8] and Morozov et al. [20] have shown that the dc and ac magnetic behaviour, respectively, of the vortex solid, measured using miniature Hall probes, are profoundly affected by polishing platelet-shaped samples into a prism-shaped cross-section. In Ref. [20], careful analysis of the ac response of the local behaviour showed that surface and geometrical barrier effects can indeed be separated in prism-shaped samples at high temperatures. Pronounced differences between platelet and prism-shaped samples have also been observed on the nonlinear transport properties of BSCCO crystals at high temperatures [10], as predicted by Benkraouda and Clem [11]. Here, we present ‘global’ magnetisation measurements on platelet, semi-ellipsoidal and prism-shaped samples using a SQUID magnetometer. Clear differences are observed in the behaviour of the different samples in the high and intermediate temperature regimes. These are discussed in terms of the competition between bulk pinning and geometrical and surface barrier effects.

## 2. Experimental

Single crystalline boules of near-optimally doped BSCCO with  $T_c \approx 89$  K were grown using an in-

frared floating zone furnace [27]. The boules were cleaved to yield single crystals with optically smooth parallel surfaces and thicknesses of several tens of microns. These were carefully cut into bars using a miniature wire saw. Pairs of bars cut from adjacent parts of the same starting crystals were selected. One of each pair was then gently mechanically polished, using  $0.25\text{ }\mu\text{m}$  diamond paste, into either a prism or a semi-ellipsoidal shape while the other retained its platelet shape. The ‘prism’ pair and the ‘ellipsoid’ pair were cut from starting material from two different boules with nominally the same doping state. A schematic representation of the sample cross-sections, normal to their long axes, is presented in Fig. 1(a). Results are shown for one prism and its bar partner and one ellipsoid and its bar partner. The dimensions of the prism and bar pair were  $1.82 \times 0.26 \times 0.06$  mm and  $1.82 \times 0.22 \times 0.06$  mm, respectively, with the angle between the sloped faces of the prism and the base (the  $ab$ -planes) close to  $25^\circ$ . The dimensions for the ellipsoid and bar pair were  $0.93 \times 0.11 \times 0.03$  mm and  $1.00 \times 0.11 \times 0.04$  mm, respectively. Thus, the cross-section of the ellipsoid is like a slightly squashed semicircle. Isothermal magnetic moment-field,  $m(H)$ , measurements were made as a function of applied field using a Quantum Design MPMS-5 magnetometer. The remnant field in the magnet was reduced by damped oscillation of the magnet and the sample was warmed to above  $T_c$  to remove any trapped flux between each measurement. The unavoidable effects of inhomogeneity in the magnetic field during measurement in the SQUID magnet were minimised by using a 3 cm scan length.

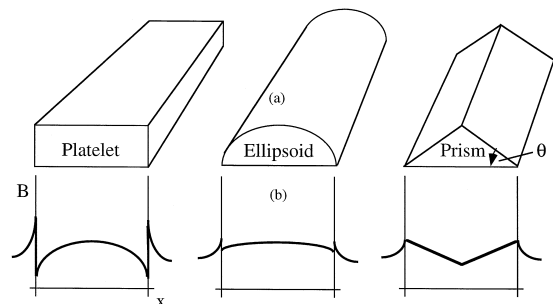


Fig. 1. (a) Schematic cross-section of the three measured sample geometries. Flux enters from the sides of the differently shaped crystals. In the prism sample,  $\theta = 25^\circ$ . (b) Schematic field profiles expected for applied fields larger than those required for full penetration are shown below each crystal.

### 3. Results and discussion

Schematic flux profiles expected [7,12,20] for the sample geometries in Fig. 1(a) are shown in Fig. 1(b) for an increasing field greater than the full penetration field. In the case of the platelet, a pronounced geometrical barrier has been shown to be dominant at high temperatures [5–12]. The GB effect causes significant hysteresis to at least  $0.5H_{c1}$  even in the absence of any bulk pinning [5,7] and the  $m(H)$  loop is usually rather flat and very similar to that observed for strong surface barriers [7,9]. In the case of the prism sample, however, the situation is rather different. The monotonically (linearly) increasing thickness of the crystal toward the sample centre means that vortices always have to increase in length as they penetrate the sample. The associated line tension energy cost as a vortex penetrates exceeds the gain in Gibbs free energy due to the shape effect. Even in the absence of bulk-pinning, vortices ‘pile up’ close to the edges and the resulting profile is similar to that expected from the Bean-model for increasing field, with a monotonically decreasing internal field toward the sample centre. Finally, for the semi-ellipsoidal, a behaviour intermediate between that for platelet and prism is expected. For a perfectly ellipsoidal sample, the gradient in vortex line energy is perfectly balanced by the gradient in its magnetic energy and this sample geometry would be a good way of examining the geometry barrier were it not technically difficult to produce such samples. On the other hand, 2D distributed surface barriers [17,18] would still be expected to act in this geometry.

Fig. 2(a) shows the measured magnetic moment as a function of applied field at 80 K for the platelet and ellipsoid pair. Both curves show the behaviour expected for a very weak pinning Type II superconducting material. A small amount of hysteresis is present at low fields but the magnetisation loops become reversible above about 60 Oe at the irreversibility field,  $H_{irr}$ , which is several orders of magnitude below the upper critical field,  $H_{c2}$ , at this temperature. A broad melting ‘step’ and change in slope of the reversible magnetisation is just visible in the data and is marked on the figure at the melting field,  $H_m$ , close to where the loops become reversible for both samples. The figure suggests that

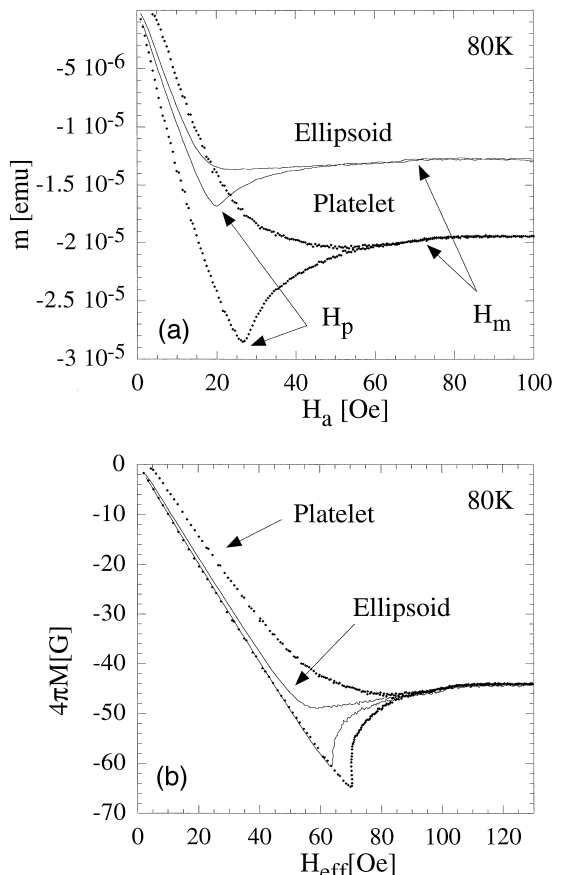


Fig. 2. (a) Magnetic moment vs. applied field at 80 K for the platelet (points) and ellipsoidal (line) crystals prepared from the same starting crystal. (b) Same as Fig. 2(a) but now the moment has been used to calculate the magnetisation and the applied field is used to calculate the average effective field (at the sample surface) by correcting for the demagnetising factor. The penetration field,  $H_p$ , is shown on the figure and is smaller for the ellipsoid, as is also the hysteresis.

the hysteresis in the ellipsoid-shaped sample is smaller than for the platelet. However, the different demagnetisation factors and sample volumes make accurate comparison difficult on such a plot. Accordingly, we calculate the volume magnetisation,  $m/V = 4\pi M$ , for the two samples and plot this as a function of the effective surface field,  $H_{eff} = H_a - 4\pi nM$ , determined by the demagnetising factor,  $n$ . Because of the small sizes of the samples and possible end effects, it is difficult to calculate demagnetisation factors accurately and we obtain the ‘effective’ value by forcing the Meissner slopes to unity.

The values thus obtained are in reasonable agreement with those expected from the sample cross-sections. Fig. 2(b) presents the data in this form. Penetration now occurs at an effective field that is more than three times higher than the applied field at which penetration occurs in Fig. 2. The slope of the Meissner region is unity and the reversible magnetisations now show good coincidence as expected. This figure demonstrates unambiguously that the penetration field and the hysteresis for the platelet sample are higher than for the ellipsoidal sample, consistent with the effect of the geometrical barrier in the platelet sample. The larger hysteresis in the platelet derives entirely from the geometry effect at these temperatures. It should be emphasised that this result precludes the introduction of bulk pinning by polishing of the ellipsoid and allows us to exclude distributed surface barriers as the mechanism controlling the hysteresis at this temperature. These would act over the whole surface of the ellipsoid-shaped sample and we would expect at least the same extent of hysteresis.

Fig. 3 presents similar data to Fig. 2(b) but for the prism and platelet pair. The prism is remarkably reversible at this temperature of 80 K as also observed in local measurements [8]. Further, the first penetration field,  $H_p$ , for the modified sample is again lower than that of the platelet. Fig. 3 shows that hysteresis is almost *completely* determined by

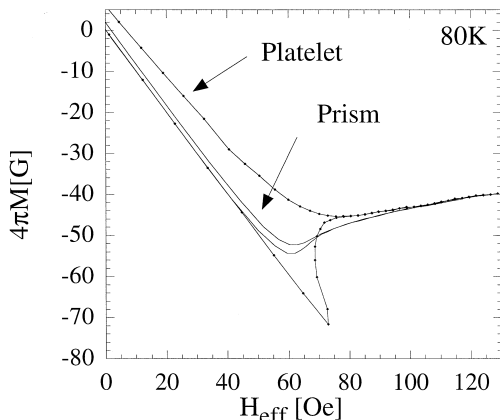


Fig. 3. Magnetisation vs. effective surface field at 80 K for the platelet and prism crystal pair prepared from the same starting crystal. It is apparent that the hysteresis is almost negligible in the case of the prism.

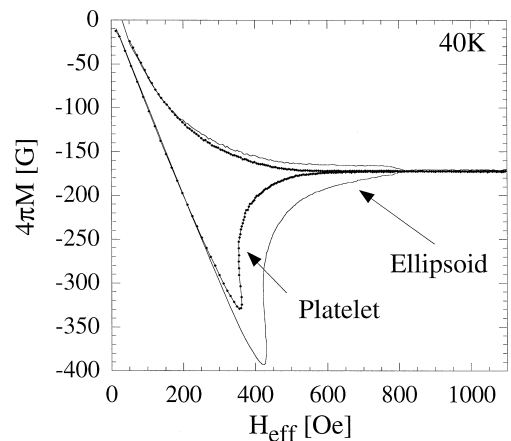


Fig. 4. Magnetisation vs. effective field at 40 K for the platelet and ellipsoid. At these lower temperatures, opposite to what is observed at higher temperatures (see Fig. 3.), the hysteresis is larger in the case of the ellipsoid.

geometrical barriers at sufficiently high temperatures in BSCCO [8]. It should also be noted that there is a small remnant moment at zero applied field when the field is decreased from its maximum. This implies that some small effect of bulk pinning does remain present, even in the prism-shaped sample. The sharp first penetration peak for the platelet sample is replaced by a rounder smoother peak for the prism. This is more similar to the form for flux penetration in strong pinning samples where vortices are pinned as soon as they enter the sample. In this case however, the bulk pinning is very weak and the magnetisation loop is almost reversible. However, the vortices are constrained from penetrating the sample by the modified shape effect.

Fig. 4 shows the behaviour of the platelet and ellipsoid pair at a lower temperature of 40 K. The penetration peaks for both samples remain rather sharp, and the remnant moments very small, indicating that bulk pinning is still rather weak, even at these lower temperatures. In contrast to what is observed at higher temperatures, the ellipsoid now displays both a larger penetration field and *larger* hysteresis than the platelet. The enhanced hysteresis persists up to the melting field and marks this feature very clearly. Similar behaviour is seen in Fig. 5, where comparable results for the prism and platelet pair are shown. This form of the hysteresis loops,

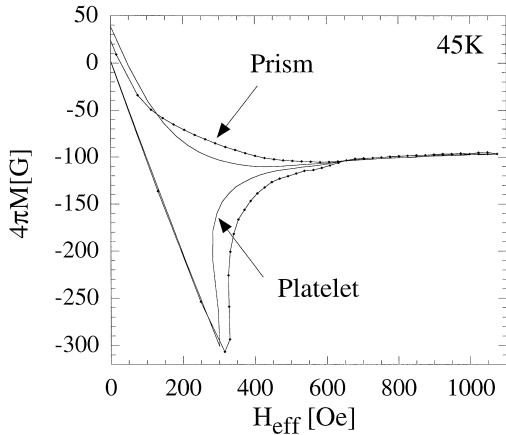


Fig. 5. Magnetisation vs. effective field at 45 K for the platelet and prism pair. The hysteresis is larger in the case of the prism than for the platelet at these lower temperatures, as also observed for the semi-ellipsoid in Fig. 4.

where they ‘pinch’ off rapidly at the melting field, is reminiscent of the observation, in BSCCO crystals [28] with a low density,  $B_\phi \approx B_{c1}$ , of columnar defects introduced by small doses of heavy ion irradiation. The matching field,  $B_\phi$ , is the field at which the average spacing of the vortices,  $a_0 = (\Phi_0/B)^{1/2}$ , is equal to the average spacing between the columnar defects. These strong-pinning columnar defects increase hysteresis substantially but only below the melting field,  $H_m$ , where the vortex lattice, because of its shear modulus,  $c_{66}$ , is able to be pinned effectively by a small number of strong pins. It would be tempting to suggest that the polishing technique used to prepare the ellipsoid and prism had therefore also introduced a small number of strong pinning sites. However, the remnant moment of the ellipsoidal sample is comparable with or even smaller than that of the platelet making this possibility less likely. On the other hand, surface barrier effects, rather than the geometrical barrier, may be dominant at these intermediate temperatures, as also suggested elsewhere [16,19,21–23]. If this were the case, one would expect, since the barriers act strongly only for flux entry in HTS [20,24], that hysteresis would only be enhanced on the *increasing* field leg. This indeed appears to be the case for the ellipsoidal sample shown in Fig. 4. The data for the prism at 45 K in Fig. 5 shows that the enhancement of hysteresis is almost the same on increasing and decreasing legs.

Therefore, we cannot preclude some contribution from polishing induced surface pinning. Although we attempted to always polish the crystal along a direction parallel to the penetrating vortices (normal to the long axis of the samples), components of scratches that are orthogonal to the field direction act to modulate the effective thickness of the crystal and therefore behave in a similar manner to the distributed surface barrier. Since vortices have to ‘penetrate’ across these scratches for both increasing and decreasing fields, this would enhance hysteresis symmetrically at fields below melting. It seems reasonable that such surface pinning may not be sufficiently strong to change the measured remnant magnetisation and would therefore be consistent with what we observe.

In order to elucidate further the origin of the enhanced hysteresis at intermediate temperatures, we have made relaxation measurements in the prism and platelet pair at the fields and temperatures where the effect is observed. Since the reversible magnetisation is large compared to the hysteresis, we measure relaxation on both increasing and decreasing (after the field has been increased to above  $H_{irr}$ ) branches of the  $m$ - $H$  hysteresis loop. The difference is calculated and represents an average time dependence of the irreversible magnetic moment eliminating the influence of the reversible moment. The data is further normalised to the hysteresis at  $t = 100$  s for comparison. Fig. 6 presents this parameter,  $\Delta m(t)/\Delta m(t = 100$  s) for the prism and platelet at 40 K and 300 Oe where the enhanced hysteresis is observed in the prism. This shows that there is pronounced relaxation in both sample geometries, with the hysteresis decreasing to half of its value at  $10^2$  s by about  $10^4$  s. It shows that the larger hysteresis in the prism sample arises because relaxation is slower in this sample than in the platelet. Chikumoto et al. [16] have made careful relaxation measurements on BSCCO crystals in a similar temperature range. They observed two regimes of relaxation at the long and short timescales, respectively. The former is argued to be due to a high current density bulk pinning mechanism while the latter, which are those we probe in our measurements at longer timescales, is shown [16] to be due to relaxation over surface barriers. Similar relaxation measurements have been made on BSCCO at low fields

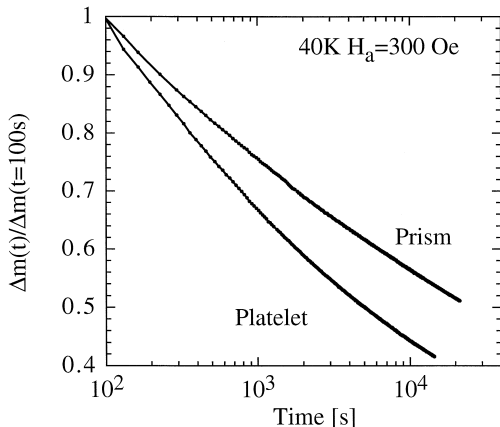


Fig. 6. Relaxation of the hysteretic magnetic moment as a function of time for the platelet and prism pair at 40 K for  $H_a = 300$  Oe.  $\Delta m = \Delta m^i - \Delta m^d$  is obtained by zero-field cooling the sample to 40 K, then ramping the field to 300 Oe and measuring the relaxation to obtain  $\Delta m^i$ . The field is then ramped above the irreversibility temperature, decreased to 300 Oe and the relaxation is measured to obtain  $\Delta m^d$ . This procedure allows the effects of the different equilibrium (reversible) moments and sample volumes to be ignored. The data is normalised at  $t = 100$  s for clarity.

by Cohen et al. [23]. They show that a single non-bulk-pinning mechanism controls the long-timescale relaxation from about 20 K up to the highest temperatures measured (about 70 K). Morozov et al. [20] have argued that a ‘distributed’ 2D surface barrier operates in BSCCO. This barrier acts at all points of a slope surface, and on each pancake that has to penetrate the sample. In the case of the platelet sample, once a stack of pancakes has entered the sample, it is no longer affected by this barrier. On the other hand, for the ellipsoidal and prism samples, the barrier acts to resist any movement of flux, since it extends, because of the polished faces, to the sample centre. This 2D surface barrier is therefore consistent with our measurements at intermediate temperatures that show greater hysteresis for the shaped samples. The temperature dependence of the penetration field provides further evidence supporting this conclusion. The (applied) first penetration field is shown in Fig. 7 for all four samples as a function of temperature on a semi-logarithmic scale. In all cases,  $H_p$  displays a clear exponential dependence on temperature in the temperature range from 40 to about 70 K. This exponential dependence has been predicted for thermal activation of vortices

across the surface barrier [17,18] and observed elsewhere [19]. At higher temperatures, the geometrical barrier becomes dominant and the temperature dependence becomes stronger as in this regime, it is determined by the temperature dependence of  $H_{cl}$ . The temperature at which the exponential behaviour no longer holds corresponds closely with that below which the geometrical barrier becomes ineffective [8,10]. It is also the temperature below which both shaped samples start to display larger hysteresis than their platelet pairs.

Finally, we have investigated whether the different sample geometries have any measurable effect on the step in the global magnetisation at the melting transition. Figs. 8(a) and (b) show the melting steps for the platelet and ellipsoidal pair, and the platelet and prism pair, respectively, at 70 K. Clearly, there are no dramatic differences in the form of the melting step within our resolution. Farrell et al. [3] have argued that the step might be an artefact of the nonuniform flux distribution in platelet-shaped samples. This idea is based on the notion that the solid phase might be able to support a pressure gradient, while the liquid cannot. In this case, even if the two phases had the same densities (and entropies), a step of nonthermodynamic origin might be expected in the locally measured magnetisation as the solid–liquid interface crossed the small Hall sensor. In this scenario, global measurements of an elliptical sample

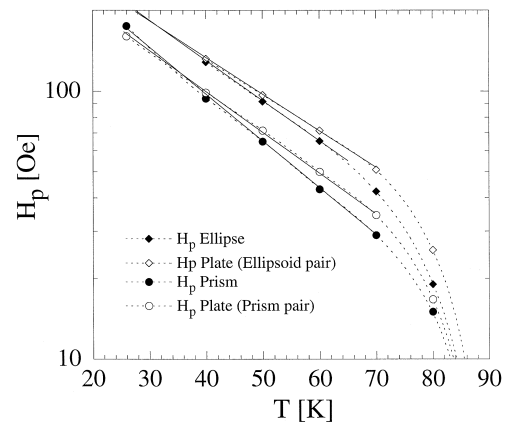


Fig. 7. Penetration fields (determined by applied and not effective field) for all the samples as a function of temperature on a semi-logarithmic plot. The solid lines indicate the regions of exponential temperature dependence.

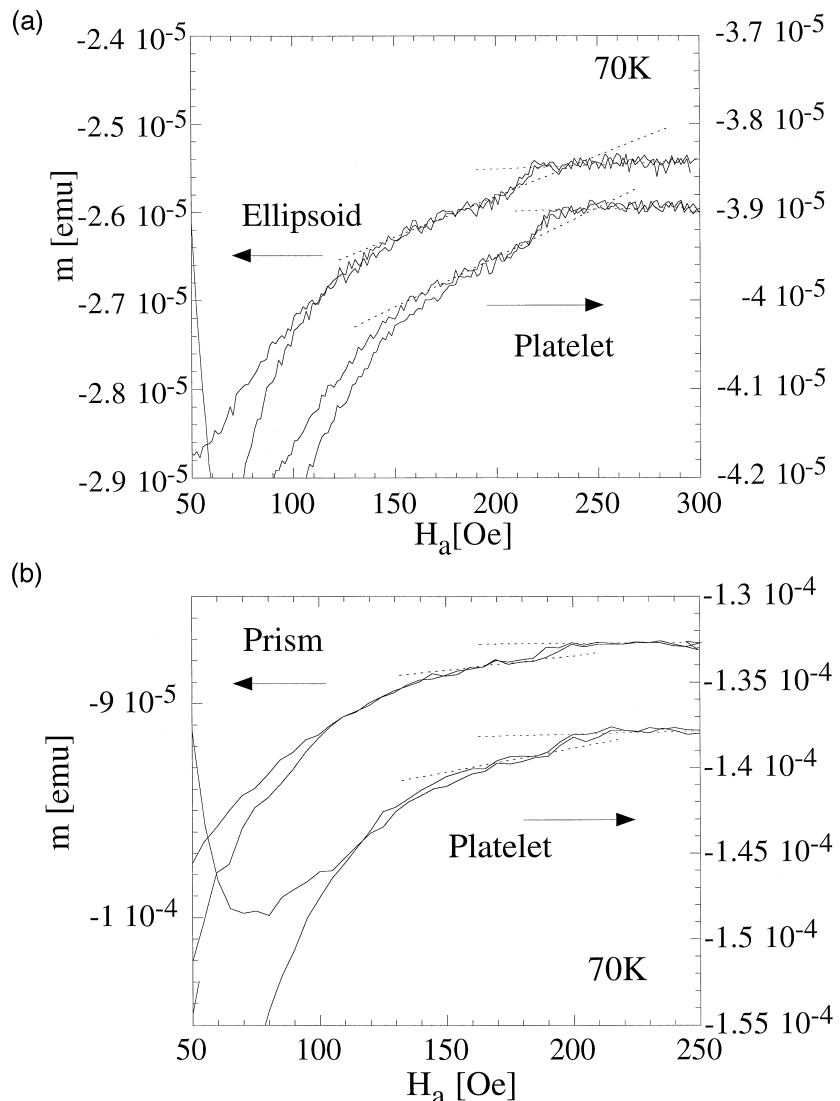


Fig. 8. (a) Expanded view of melting jumps for ellipsoid and platelet at 70 K. No significant difference can be resolved. (b) Same as (a) but comparing the prism and platelet pair.

should show no transition. Even in nonellipsoidal samples, the transition should be smeared or suppressed relative to the platelet geometry, provided that the internal field is more uniform than in platelet-shaped samples. However, the results here show that there is no observable suppression of the step. Accordingly, they support the opposite conclusion that the step indeed has a thermodynamic rather than a nonequilibrium origin. The size of the steps is used to calculate the change in flux density  $B$ , which

is found to be close to 0.6 G for both samples, in agreement with other measurements [3].

#### 4. Conclusions

We have produced samples of different shapes to assess the effect on the global magnetisation. These results show that hysteresis in the magnetisation of BSCCO at temperatures above  $\approx 70$  K is deter-

mined almost entirely by shape rather than surface effects. At intermediate temperatures, the shaped samples display greater hysteresis than the platelet samples. Because there is no significant increase in bulk pinning (which might have been introduced by polishing), we suggest that the hysteresis in this temperature range is controlled by surface barriers, in agreement with other measurements reported elsewhere. The different sample shapes display no apparent differences of the melting step, consistent with a thermodynamic origin for this feature. These results emphasise the danger of extracting (bulk) pinning properties from magnetisation curves of platelet-shaped crystals with low levels of bulk pinning.

### Acknowledgements

RAD is grateful to the Royal Society for Support. This work is partly supported by Grant-in-Aid for Scientific Research from the Ministry of Education, Science, Sports and Culture, Japan.

### References

- [1] G. Blatter, M.V. Feigel'man, V.B. Geshkenbein, A.I. Larkin, V.M. Vinokur, Rev. Mod. Phys. 66 (1994) 1125.
- [2] V. Vinokur, B. Khaykovich, E. Zeldov, R.A. Doyle, M. Konczykowski, P.H. Kes, Physica C 295 (1997) 209.
- [3] D.E. Farrell, E.J. Halperin, L. Klein, P. Fournier, A. Kapitulinik, E.M. Forgan, A.I.M. Rae, T.W. Li, M.L. Trawick, R. Sasik, J.C. Garland, Phys. Rev. B 53 (1996) 11807.
- [4] C.D. Dewhurst, R.A. Doyle, Phys. Rev. B 56 (1997) 10832.
- [5] T.B. Doyle, R. Labusch, R.A. Doyle, Physica C 290 (1997) 148.
- [6] M.V. Indenbom, G. D'Anna, M.-O. Andre, W. Benoit, H. Kronmuller, T.W. Li, P.H. Kes, in: H.W. Weber (Ed.), Proc. 7th Int. Workshop on Critical Currents in Superconductors, World Scientific, Albach, Austria, Jan. 1994, p. 327.
- [7] E. Zeldov, A.I. Larkin, V.B. Geshkenbein, M. Konczykowski, D. Majer, B. Khaykovich, V.M. Vinokur, H. Shtrikman, Phys. Rev. Lett. 73 (1994) 1428.
- [8] D. Majer, E. Zeldov, M. Konczykowski, Phys. Rev. Lett. 75 (1995) 1166.
- [9] A.V. Kuznetsov, D.V. Eremenko, V.N. Trofimov, Phys. Rev. B 57 (1998) 5412.
- [10] R.A. Doyle, S.F.W.R. Rycroft, T.B. Doyle, E. Zeldov, T. Tamegai, S. Ooi, Phys. Rev. B 53 (1998) 135.
- [11] M. Benkraouda, J.R. Clem, unpublished.
- [12] M. Benkraouda, J.R. Clem, Phys. Rev. B 53 (1996) 5716.
- [13] E.H. Brandt, Rep. Prog. Phys. 58 (1995) 1465.
- [14] C.J. van der Beek, M.V. Indenbom, G. D'Anna, W. Benoit, Physica C 258 (1996) 105.
- [15] V.N. Kopylov, A.E. Koshelev, I.F. Schegolev, T.G. Togonidze, Physica C 170 (1990) 291.
- [16] N. Chikumoto, M. Konczykowski, N. Motohira, A.P. Malozemoff, Phys. Rev. Lett. 69 (1992) 1260.
- [17] L. Burlachkov, Phys. Rev. B 47 (1993) 8056.
- [18] L. Burlachkov, V.B. Geshkenbein, A.E. Koshelev, A.I. Larkin, V.M. Vinokur, Phys. Rev. B 50 (1994) 16770.
- [19] E. Zeldov, D. Majer, M. Konczykowski, A.I. Larkin, V.M. Vinokur, V.B. Geshkenbein, N. Chikumoto, H. Shtrikman, Europhys. Lett. 30 (1995) 367.
- [20] N. Morozov, E. Zeldov, M. Konczykowski, R.A. Doyle, Physica C 291 (1997) 113.
- [21] D.T. Fuchs, E. Zeldov, M. Rappaport, T. Tamegai, S. Ooi, H. Shtrikman, Nature 391 (1998) 373.
- [22] D.T. Fuchs, E. Zeldov, T. Tamegai, S. Ooi, M. Rappaport, H. Shtrikman, Phys. Rev. Lett. 80 (1998) 4971.
- [23] L.F. Cohen, J.T. Totty, G.K. Perkins, R.A. Doyle, K. Kadouaki, Supercond. Sci. Technol. 10 (1997) 195.
- [24] M. Konczykowski, in: M. Baran, W. Gorzkowski, H. Szymczak (Eds.), Proc. Int. Workshop on Critical Current Limitations in High Temperature Superconductors, Zaborow, Poland, World Scientific, 1991.
- [25] E.H. Brandt, unpublished.
- [26] R. Labusch, T.B. Doyle, Physica C 290 (1997) 143.
- [27] N. Motohira, K. Kuwahara, T. Hasegawa, K. Kishio, K. Kitazawa, J. Ceram. Soc. Jpn. (Int. Ed.) 97 (1989) 994.
- [28] B. Khaykovich, M. Konczykowski, E. Zeldov, R.A. Doyle, P.H. Kes, D. Majer, T.W. Li, Phys. Rev. B 56 (1997) R517.